



HIGH RESOLUTION FABRY-PÉROT INTERFEROMETER – DYNAMIC SYSTEM MODELING AND NANOPositionING CONTROL SYSTEM DESIGN USING LQG/LTR TECHNIQUE

Ana María Molina Arcila

Fábio de Oliveira Fialho

Laboratório de Automação e Controle – Departamento de Telecomunicações e Controle da Escola Politécnica da Universidade de São Paulo – Avenida Professor Luciano Gualberto. Trv. 3, nº 158, São Paulo, Brasil

ammolina@usp.br

fabio.fialho@usp.br

Fernando Orsatti

Laboratório de Automação e Controle – Departamento de Telecomunicações e Controle da Escola Politécnica da Universidade de São Paulo – Avenida Professor Luciano Gualberto. Trv. 3, nº 158, São Paulo, Brasil

fernando.orsatti@oepe.com.br

Victor Atílio Marchiori

Laboratório de Automação e Controle – Departamento de Telecomunicações e Controle da Escola Politécnica da Universidade de São Paulo – Avenida Professor Luciano Gualberto. Trv. 3, nº 158, São Paulo, Brasil

victoratilio@usp.br

Issa Ouattara

Laboratoire d'Astrophysique de Marseille – 38, rue Frédéric Joliot-Curie, Marseille, France

issa.ouattara@oamp.fr

Leonardo Pinheiro da Silva

Laboratório de Automação e Controle – Departamento de Telecomunicações e Controle da Escola Politécnica da Universidade de São Paulo – Avenida Professor Luciano Gualberto. Trv. 3, nº 158, São Paulo, Brasil

leonardo.pinheiro@oepe.com.br

Jair Pereira de Souza

Laboratório de Microeletrônica – Departamento de Engenharia de Sistemas Eletrônicos da Escola Politécnica da Universidade de São Paulo – Avenida Professor Luciano Gualberto. Trv. 3, nº 158, São Paulo, Brasil

jpsouza@lme.usp.br

Claudia Lucia Mendes de Oliveira

Instituto de Astronomia, Geofísica e Ciências Atmosféricas da Universidade de São Paulo – Rua do Matão, nº 1226, São Paulo, Brasil

oliveira@astro.iag.usp.br

Abstract. *In this paper, we present the design of the mirror nanopositioning controller of the state-of-the-art Fabry-Pérot interferometer to be installed in the Brazilian Tunable Filter Imager (BTFI) on the Southern Astrophysical Research (SOAR) telescope in Chile. The three-input-three-output multivariable (MIMO) Fabry-Pérot system is composed of three high-range Amplified Piezoelectric Actuators (APA) of 230 μm stroke and three 400 μm -range capacitive measurement systems. Its positioning control system is specified to achieve a maximum steady-state noise of 3nm rms. A sixth-order non-minimum phase complete system model was built on top of a second-order piezoelectric actuator model with hysteresis effect compensation. The multivariable robust controller was designed following the Linear Quadratic Gaussian/Loop Transfer Recovery (LQG/LTR) method. The built controller was validated in the real system and its performance was compared against a proportional-integral (PI) controller as benchmark. Simulation results show that the control algorithm is valid.*

Keywords: *Dynamic Modeling, Multivariable Systems, Robust Controller, Fabry-Pérot Interferometer, Nanopositioning Systems.*

1. INTRODUCTION

The Brazilian Tunable Filter Imager (BTFI) is a highly versatile, new technology, tunable optical imager to be used both in seeing-limited mode and at higher spatial fidelity using the SAM Ground-Layer Adaptive Optics facility (SOAR Adaptive Module) which is being deployed at the SOAR telescope. The BTFI employs Fabry-Perót interferometers in order to achieve high spectral resolutions up to $R \sim 30,000$ (Oliveira et al, 2013).

A scanning process is required to provide 2D-images within a given spectral band using a Fabry-Perót interferometer. Such process is implemented by changing the distance between its two highly reflective parallel mirrors. Current Fabry-Perót interferometers are designed to work in a fixed spectral resolution and allow for an initial adjustment of the distance between the mirrors in a range of $10 \mu\text{m}$ with a scan range of $2 \mu\text{m}$. The proposed Fabry-Perót interferometer is designed to work in a larger range of spectral resolutions ($R \sim 1000$ to $R \sim 30000$), which requires a range for the distance between the plates from zero to at least $200 \mu\text{m}$. To meet such specific requirement, high-excursion piezoelectric actuators (APA400MML, manufactured by CEDRAT Technologies Co) and high-sensitivity capacitive sensors compose the feedback nanopositioning system. Such feedback control system is needed to set and control the desired distance between the plates and is the aim of this work to develop different approaches to the design of a successful controller for the BTFI Fabry-Perót system.

For the purpose of designing the control system, a parametric second-order model of the piezoactuator was created for the specific stack actuator APA400MML. The parametric sixth-order model of the Fabry-Perót interferometer was created on top of the piezoactuator model. The result is a linear, time invariant model of the system.

With the parametric model of the Fabry-Perót system, the linear quadratic Gaussian with loop transfer recovery LQG/LTR robust MIMO (multiple input multiple output) controller design technique, presented in Athans (1986), was applied. This technique was chosen because it ends with a robust controller, able to reject disturbances and reject noise measurement with stability guaranteed in its entire range of operation. Another approach implemented for the controller was using the classic Proportional-Integral SISO (single input single output) design.

The paper is organized in the following way: Section 2 describes the instrumentation and physical configuration of the device, followed by a description of the parametric second-order model of the piezoactuators and the sixth-order model of the Fabry-Perót interferometer (Section 3). The control problem is introduced in Section 4, and the control design is presented in Section 5. The simulated and experimental results are presented in Section 6 and 7. Finally, the results are discussed in Section 8.

2. FABRY-PERÓT INSTRUMENT

The Fabry-Perót interferometer is composed of two parallel highly reflecting circular glass plates (commonly referred as the mirrors, or etalon). One plate is mounted firmly in a cylindrical mechanical system that comprises the body of the Fabry-Perót interferometer, and the second one is mounted on the same cylinder through three piezoelectric actuators (or piezoactuators), used for fine-positioning the mirrors. The piezoactuators APA400MML are solid-state long-stroke actuators based on the expansion of the active material and on a mechanism to amplify the displacement (CEDRAT 2013), allowing a maximum displacement of $250 \mu\text{m}$ at 150 V . Three capacitive sensors measure the distance between the two plates of the interferometer for feedback, with sub-nanometer resolution. Such capacitive sensors are MCC10HS ones, which have metal-resin technology and triaxial technology manufactured by FOGALE Nanotech Company.

Each of the three MCC10HS is fixed to the Fabry-Perót mount and the measurement target of each piezoactuator is fixed to the upper mirror of the etalon. In this way the sensors always measure the distance between the upper mirror and the fixed position of the sensor. The offset between the sensor fixed position and the bottom mirror is corrected a priori.

The outputs of the capacitive sensors are connected directly to MC900 modules. Such modules convert the capacitance of the sensors measure into a voltage value that is proportional to the measured distance. The modules output varies from 0 to 10 volts and the sensitivity can be calibrated based on the desired measurement range. The bandwidth of the MC900 modules is set and fixed in 10 kHz .

A picture of the Fabry-Perót etalon and the complete instrumentation of the system is shown in Fig. 1.

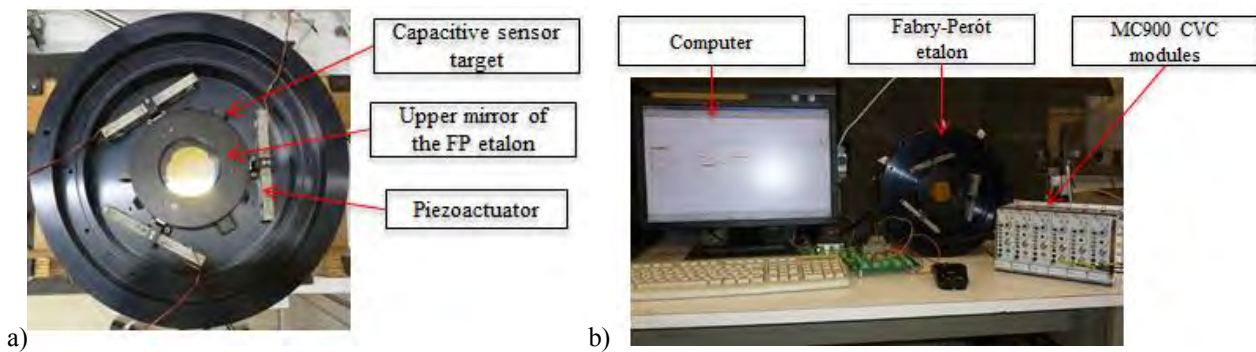


Figure 1. (a) Fabry-Perot upper mirror and piezoactuators. There is one measurement target between two piezoactuators, separated 60 degrees each. (b) Fabry-Perot control system instrumentation.

3. FABRY-PERÓT MODEL

3.1 Piezoactuator second-order model

The overall mechanical behavior of the piezoactuator practically equals that of a single mass-spring-damper system (Adriaens et al., 2000). The differential equation used in the model of the piezoactuator system, is the well-known general differential equation for linear time invariant second-order systems written as:

$$m\ddot{y} + c\dot{y} + ky = c\dot{u} + ku \quad (1)$$

Where y and u represent the actuator displacement and input voltage, respectively. The effective mass m , in Eq. (2) is a function of the natural frequency Wn , and the stiffness of the piezoactuator k , which is specified in the piezoactuator datasheet (CEDRAT TECHNOLOGIES, 2013).

$$m = \frac{k}{Wn^2} \quad (2)$$

The damping coefficient c , is calculated as in Eq. (3):

$$c = 2m\zeta Wn \quad (3)$$

where ζ is the damping coefficient, calculated as a function of the gain P , of the natural frequency Wn , as shown in Eq.(4). Both P and Wn are inferred from the piezoactuator frequency response.

$$\zeta = \sqrt{\frac{1}{4(P^2 - 1)}} \quad (4)$$

These equations are applied to the three piezoactuators of the system; therefore m_1 , c_1 , and k_1 refer to these variables in piezoactuator 1; m_2 , c_2 and k_2 to the variables in piezoactuator 2; and m_3 , c_3 and k_3 for piezoactuator 3. A small time delay τ was introduced to the model to give a good fit to the phase curve of the real system frequency response in Fig. 3.

After Laplace transformation of Eq. (1) the transfer function of the piezoactuator can be written as:

$$\frac{Y(s)}{U(s)} = \frac{cs + k}{ms^2 + cs + k} e^{-\tau s} \quad (5)$$

3.2 Identification of the piezoactuator second-order model

To build a model for the piezoactuators, the frequency response of the system was taken using a Dynamic Signal Analyzer (DSA HP35665A), where a sinusoidal input signal of 1 V of amplitude over the frequency range of interest (1 Hz to 3 kHz) was applied to the piezoactuator. The resulting low displacement of the piezoactuator ($\pm 1 \mu\text{m}$), in the z direction as shown in Fig. 2, was measured by the capacitive sensors and fed back to the DSA.

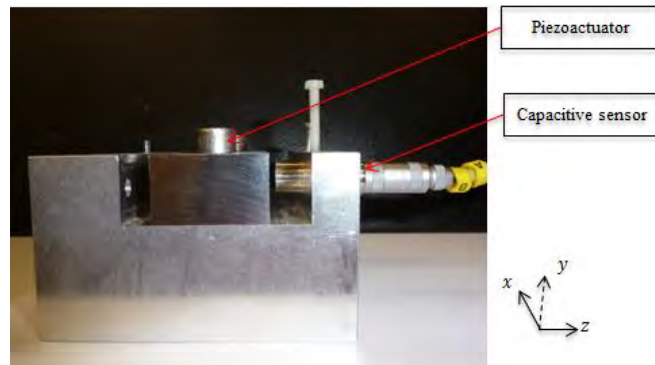


Figure 2 Test bench setup for the acquisition of the piezoactuator dynamic response.

The frequency response of the piezoactuator is plotted as a Bode plot shown in Fig. 3. The parameters P and W_n of the piezoactuators model were taken from this Bode plot, were P has a value of -5 dB and W_n has a value of 655 Hz.

The Bode plot of the transfer function of Eq. (5) is also shown in Fig. 3 (dashed red line). The system only shows one peak, while experimental results (solid black line) indicate that there are more peaks and valleys in between every two peaks. As stated by Adriaens et al. (2000), there can be infinite peaks and valleys because the mass of the piezoactuator is not concentrated in some points, as in linear mass-spring-damper systems of arbitrary order, but distributed over the element. Considering this, the model presented here is a good approximation up to the first natural frequency and such limitation imposes a constraint to the design of the control law (Sec. 5). In practice, as stated by Bashas et al. (2007), the working frequency of the piezoactuator barely exceeds its first natural frequency. Therefore, the distributed parameters nature of the piezoactuator could be safely neglected and the model could be reduced to a lumped parameter representation, especially when integrated with flexural mechanical compartments.

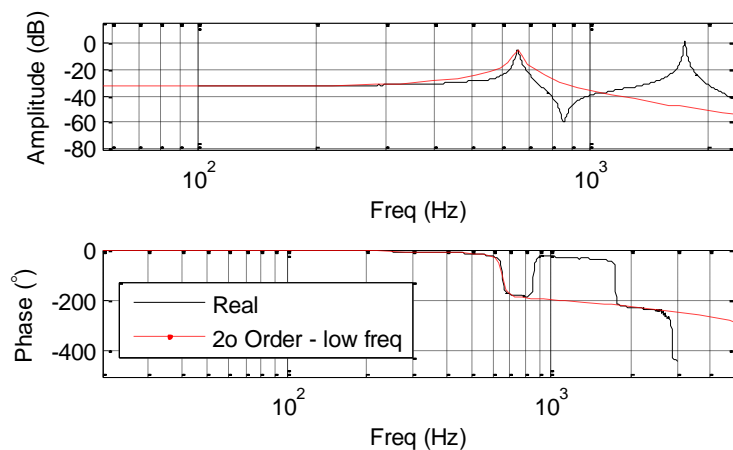


Figure 3 APA400MML piezoactuator frequency response. The solid black line represents the experimental frequency response taken with a Dynamic Signal Analyzer. The dashed red line is the Bode plot of the second order model.

3.3 Fabry-Perót sixth-order model

A sixth-order parametric model for the Fabry-Perót system, which is composed of three piezoactuators coupled with the mirror mass, was built on top of the previously presented model for the piezoactuator. The input of the MIMO system are the three piezoactuators voltage inputs, u_1 , u_2 and u_3 , and the outputs are the measurement of the capacitive sensors, s_{12} , s_{23} , s_{13} , all of them in Volts.

The model takes into account the geometrical position of the sensors. The measurement targets of the sensors are placed 60 degrees from each of the piezoactuators, as shown in Fig. 4b. The graphical representation of the system is shown in Fig. 4a.

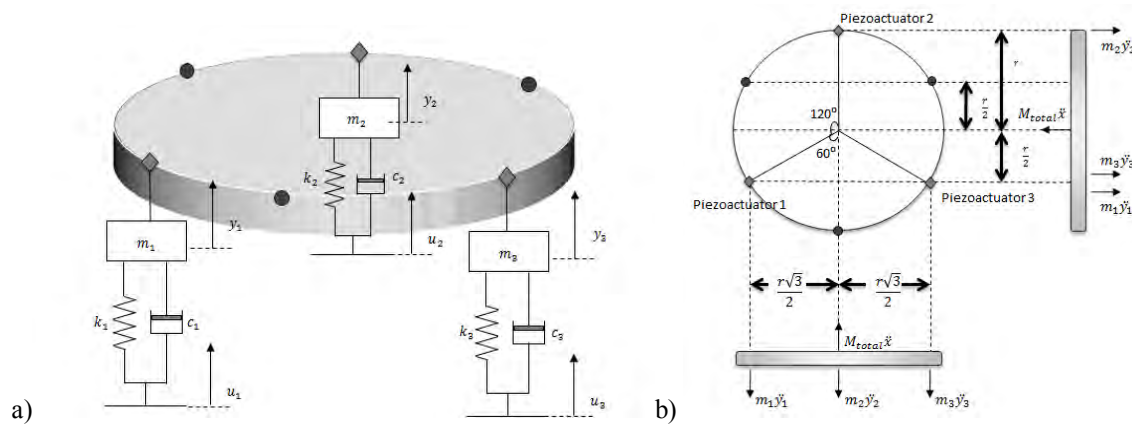


Figure 4. a) Schematic of the Fabry-Perot instrument. The disk represents the upper mirror, the mass-spring-damper systems represent the piezoactuators, and the dots on the disk represent the capacitive sensors measurement targets. b) Fabry-Perot system geometrical representation and force diagram.

The total mass of the system is the sum of the masses of the mirror plate and the effective masses of the piezoactuators second order model, as stated in Eq. (6).

$$M_{total} = m_{mirror} + m_1 + m_2 + m_3 \quad (6)$$

Taking x as the total displacement of the mirror plate, the force-balance equation, applying the expression of Eq. (1) for every piezoactuator results in:

$$M_{total}\ddot{x} = -k_1y_1 - k_2y_2 - k_3y_3 - c_1\dot{y}_1 - c_2\dot{y}_2 - c_3\dot{y}_3 + k_1u_1 + k_2u_2 + k_3u_3 + c_1\dot{u}_1 + c_2\dot{u}_2 + c_3\dot{u}_3 \quad (7)$$

The moment of force for the plate in the y axis is:

$$I_y\ddot{\theta}_y = -[k_1(y_1 - u_1) + c_1(\dot{y}_1 - \dot{u}_1)]\frac{r\sqrt{3}}{2} + [k_3(y_3 - u_3) + c_3(\dot{y}_3 - \dot{u}_3)]\frac{r\sqrt{3}}{2} \quad (8)$$

Similarly, the moment of force for the plate in the z axis is:

$$I_z\ddot{\theta}_z = -[k_1(y_1 - u_1) + c_1(\dot{y}_1 - \dot{u}_1)]\frac{r}{2} + [k_2(y_2 - u_2) + c_2(\dot{y}_2 - \dot{u}_2)]r - [k_3(y_3 - u_3) + c_3(\dot{y}_3 - \dot{u}_3)]\frac{r}{2} \quad (9)$$

The distance output in the location of the capacitive sensors measurement targets:

$$s_{12} = x + \theta_y \frac{r\sqrt{3}}{2} - \theta_z \frac{r}{2} \quad (10)$$

$$s_{23} = x - \theta_y \frac{r\sqrt{3}}{2} - \theta_z \frac{r}{2} \quad (11)$$

$$s_{13} = x + \theta_z r \quad (12)$$

Finally, the space state representation is given by Eq. (13) and Eq. (14), with the matrix **A**, **B**, **C**, **D** defined as in Appendix 1a. The result is a linear and time-invariant (LTI) model with 3 controls, 3 outputs and 6 state variables.

$$\dot{x} = \mathbf{A}x + \mathbf{B}u \quad (13)$$

$$y = \mathbf{C}x + \mathbf{D}u \quad (14)$$

This space state representation can be transformed to a transfer function representation for each input/output relation.

The transfer functions for the Fabry-Perot system are showed in Appendix 1b.

3.4 Identification of the Fabry-Perót model

As in the modeling of the piezoactuators, presented in section 3.1, the frequency response of the system was taken for every input and output combination using the same dynamic signal analyzer, in the range of frequency of interest (1 Hz – 1 kHz). The Bode plots for each input and output combination are shown in Fig. 5.

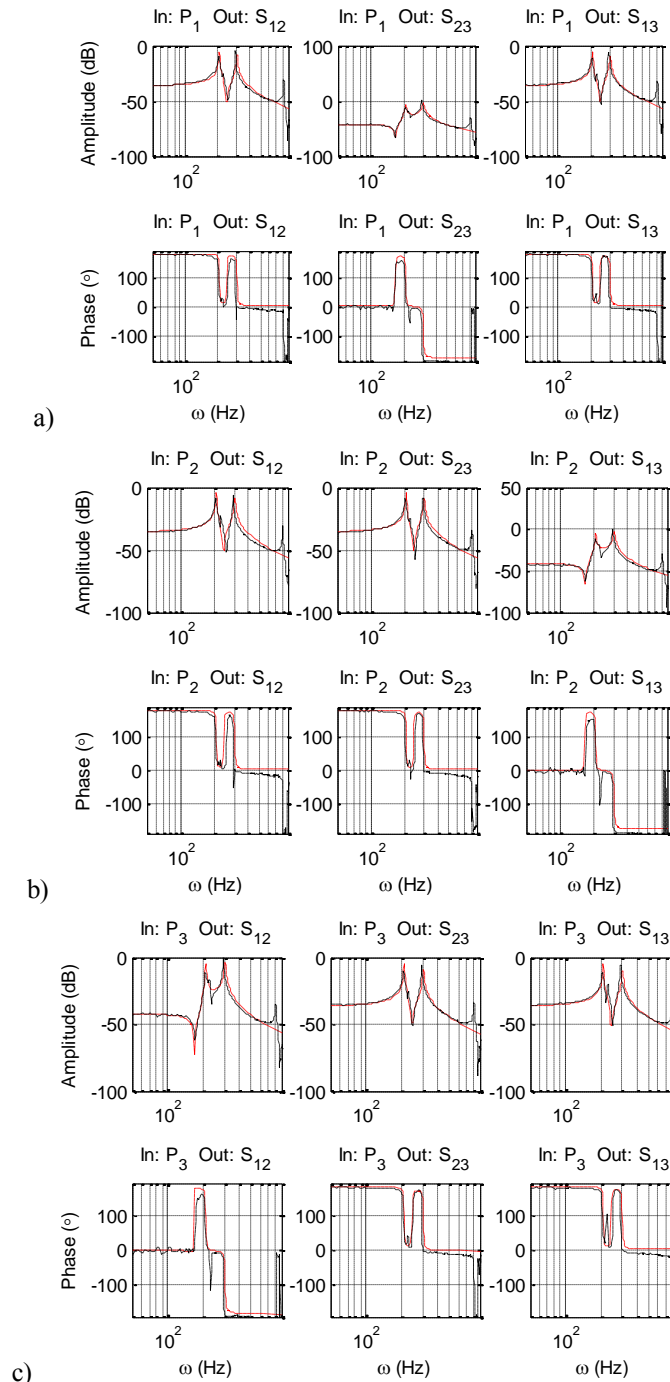


Figure 5 Bode plot of the Fabry-Perót system when exciting only one input. a) Input signal only in u_1 , b) Input signal only in u_2 , c) Input signal only in u_3 . Solid black line is the Bode plot of the parametric model. Dashed red line is the real response of the system.

The presented model has limitations because some important effects, like hysteresis, creep, temperature and humidity, were not taken into account in order to simplify the modeling of the system allowing the use of linear control techniques like the LQG/LTR controller design. Nevertheless, an ongoing work (Atilio et al, 2013) that drives the piezoactuators by charge instead of voltage to eliminate the hysteresis and creep effects will make the linear dynamical model proposed here very close to the real system.

3.5 The Fabry-Perót modelling error

With the frequency response presented in Fig. 5 it was possible to calculate the modeling error EM , using the following multiplicative error formula on the acquired data points:

$$EM(s) = [G_R(s) - G_N(s)]G_N(s)^{-1} \quad (15)$$

Where G_R is the transfer function of the real plant and G_N is the nominal model of the system.

This representation for the error was adopted because it describes the error, reflected in the plant output, in the modeling of the plant transfer function as well as the error in the loop transfer function (Da Cruz, 1996).

Next, the frequency response of the inverse of the modeling error of Eq. (16) was taken, as presented in Fig. 6. This helped in the analysis of how well the model represents the system as a function of the frequency and is also needed for the LQG/LTR design method, which will be presented in the next section.

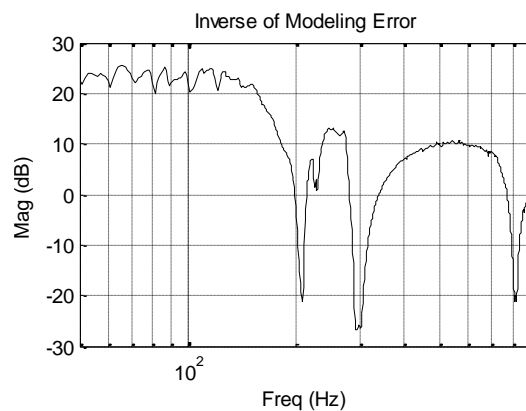


Figure 6 Fabry-Perót system multiplicative modeling error

Fig. 6 shows high-frequency modeling errors which impose a limit to the control system bandwidth, limiting the performance of the feedback system (Athans, 1986). For the current model of the system, the crossover frequency is on 200 Hz, which is taken into account in the robust control design in section 5.2.

4. FABRY-PERÓT CONTROL PROBLEM

4.1 Main operation mode

The main operation mode of the Fabry-Perót instrument is the scanning one, which consists in varying the distance between the mirrors of the interferometer, between one distance position to another, and going the way back, in n steps. This is repeated for a number m of times creating a sequence of ladders.

4.2 Performance specifications

The performance specifications for the feedback control system in scanning mode are the following:

1. Follow the reference (small steps) signal with null steady state average error, and steady state maximum standard deviation of 3nm rms.
2. Reject disturbances up to 100 Hz.

Finally, step response overshoots must be minimized in order to maximize the instrument operation range.

5. CONTROL SYSTEM DESIGN

5.1 Proportional-Integral Compensator

As a benchmark, and due to its simplicity of implementation and satisfactory performance on following step references with zero steady-state error, a simple Proportional Integral (PI) controller of the form of Eq. (16) has been implemented.

Ana María Molina Arcila, Fábio de Oliveira Fialho, Fernando Orsatti
High Resolution Fabry-Pérot Interferometer – Dynamic System Modeling And Nanopositioning Control System Design

$$K_{PI} = kp + ki \frac{1}{s} \quad (16)$$

Where kp is the proportional constant, ki is the integral constant and s is the Laplace complex angular frequency.

The PI compensator for the FP is assumed to be an ensemble of three SISO (single input single output) uncoupled control loops stated by G_{11} , G_{22} , G_{33} transfer functions as in Appendix 1.b.

Coupling transfer functions of the system defined by G_{12} , G_{23} , G_{13} are neglected, meaning that we only consider the mass of glass over the actuators, not the coupling force provoked by the circular mirror over the three piezoactuators.

The same compensator, K_{PI} , was used for the three SISO systems.

Experimental tuning has been chosen as the methodology for the PI parameters tuning.

5.2 Linear quadratic Gaussian with loop transfer recovery compensator.

The system is assumed to be linear in order to be able to design a robust controller.

The main characteristics of the LQG/LTR robust controller are that it has nominal stability and stability-robustness to modeling errors while achieving good performance (Athans, 1986).

The goal is to design a MIMO LQG/LTR compensator, $K(s)$, for this model to meet the performance specifications presented in Section 4.2. For this purpose, three integrators, one for each input channel of the plant, were added to the Design Plant Model (DPM) in order to achieve null steady-state error to a step input. Also, and considering that a typical step size for the scanning mode is of 10 nm, the controller was set to have a noise-signal ratio smaller than 30%, in order to achieve a steady state maximum standard deviation of 3 nm. And, lastly, the bandwidth of the closed loop system was set beyond 100 Hz in order to reject disturbances up to this frequency.

The model of the Fabry-Perót instrument, presented in section 3.3, includes 6 state variables. The resultant MIMO compensator will then have 12 states (6 states from the original system model + 3 integrators of the DPM + 3 integrators included in the controller) and will be given by:

$$K(s) = \mathbf{G}(s\mathbf{I} - \mathbf{A} + \mathbf{B}\mathbf{G} + \mathbf{H}\mathbf{C})^{-1}\mathbf{H} \quad (17)$$

Where \mathbf{A} , \mathbf{B} and \mathbf{C} are the matrices of the space state representation of the system model, as defined in the Appendix 1a, \mathbf{G} is the gain matrix of the controller and \mathbf{H} is the Kalman Filter observer gain matrix, both defined as in Appendix 2.

6. SIMULATION RESULTS

6.1 Proportional-Integral compensator simulation results

Figure 7 shows the block diagram of the PI control loop simulation:

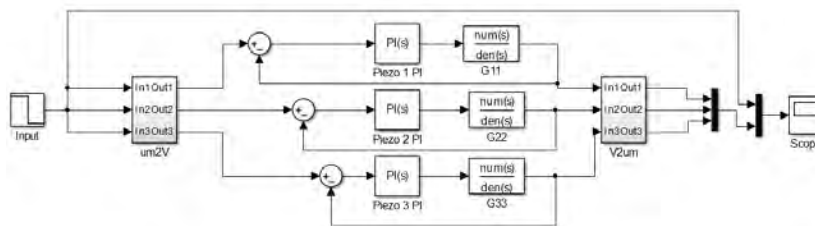


Figure 7 Unity feedback configuration for the PI controller of the Fabry-Perót system.

And the simulation results for a step input signal of 5 μm is shown in Fig. 8.

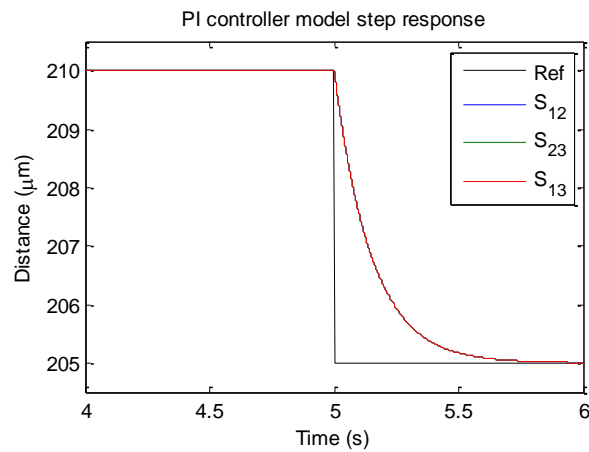


Figure 8 Fabry-Perót model step response with PI controller simulation

As it can be seen in the figure, the outputs of the system do not present overshoot in the dynamic response and follow the reference with null steady state error, achieving the performance requirements.

6.2 LQG/LTR compensator simulation results

The robust controller simulation block diagram is as shown in Fig. 9.

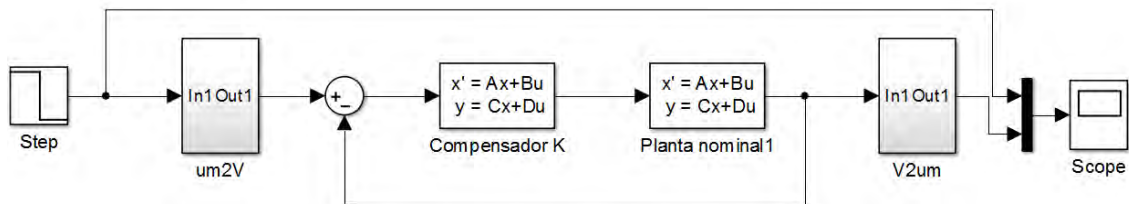


Figure 9 Robust controller simulation block diagram

The simulation results for a step input signal of $5\mu\text{m}$ is shown in Fig. 10.

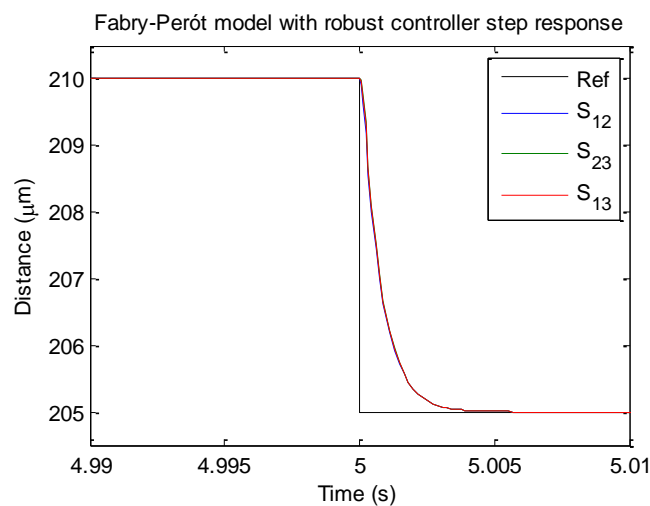


Figure 10 Fabry-Perót system step response with robust controller

The outputs of the system do not present overshoot in the dynamic response and follow the reference with null steady state error, achieving the performance requirements.

7. EXPERIMENTAL VALIDATION OF COMPENSATORS

For the experimental validation of the compensators in the real system, the simulations presented in Fig. 7 and 9 are run in real time using a sample frequency of 4500 Hz. The digital to analog interface between the computer and the piezoactuators, and the analog to digital conversion between the MC900 output and the computer, is done by two data acquisition boards, NI 6221.

7.1 Proportional-Integral compensator experimental results

The experimental results for a step input signal of $5\mu\text{m}$ is shown in Fig. 11.

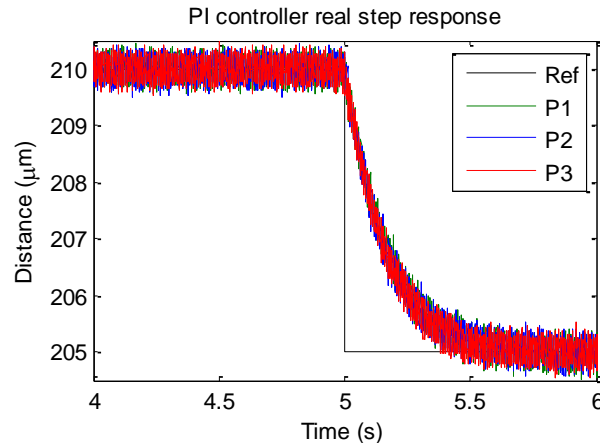


Figure 11 Fabry-Perót system step response with PI controller

As it can be seen in the figure, the outputs of the system do not present overshoot in the dynamic response and follow the reference with null steady state error. However, the output signals of the system, acquired by the data acquisition boards, present a steady-state standard deviation of 140 nm. The source of this noise was studied, reaching the conclusion that the noise is introduced by the computer and the data acquisition boards, which will not be part of the system once the control algorithm is implemented in an isolated controller board in the future. For this reason, the noise specification used for the validation is the relative specification of noise-signal ratio of 0.3.

For these experimental results, the signal has a steady state standard deviation of $0.140\mu\text{m}$ for a $5\mu\text{m}$ mean step signal, resulting in a noise-signal ratio of 0.03.

7.2 LQG/LTR compensator experimental results

The experimental validation of the LQG/LTR robust controllers with hysteresis compensation is part of our current work. For the final version of this paper we are planning to show the results of this validation.

8. CONCLUSIONS

This paper has proposed a linear time-invariant second-order model for the amplified piezoactuator APA400MML and a sixth-order LTI model for the Fabry-Perót system of the BTFI instrument. These models were used to design a PI and a robust LQG/LTR nanopositioning controllers for the Fabry-Perót system.

The simulation and implementation results of the controllers have verified the effectiveness of the proposed control schemes, demonstrating that they can achieve a fast and smooth reference following response, rejecting disturbances up to 100 Hz and having a satisfactory noise-signal ratio.

9. ACKNOWLEDGEMENTS

We would like to thank the Laboratório de Microeletrônica do Departamento de Sistemas Eletrônicos of the Universidade de São Paulo for their support and for sharing their space and resources with us. The first author would also like to thank the Fundação de Amparo a Pesquisa do Estado de São Paulo, FAPESP, process number 2011/11877-5 for financial support.

10. REFERENCES

- Adriaens, H. J. M. T. S., Willem L. De Koning, and Reinder Banning. "Modeling piezoelectric actuators." *Mechatronics*, IEEE/ASME Transactions on 5.4 (2000): 331-341.
- Athans, Michael. "A tutorial on the LQG/LTR method." American Control Conference, 1986. IEEE, 1986.
- CEDRAT TECHNOLOGIES, 2010. "Technical Datasheet APA400MML". 1 May 2010
http://www.cedrat_technologies.com/fileadmin/user_upload/cedrat_groupe/Mechatronic_products/Piezo_actuators_electronics/APAs/APA400MML_GB_v3.3.pdf
- CEDRAT TECHNOLOGIES, 2013. "CEDRAT TECHNOLOGIES Piezo Products Catalog Version 4.1"
- de Oliveira, Cláudia Mendes, et al. "The Brazilian Tunable Filter Imager for the SOAR Telescope." *Publications of the Astronomical Society of the Pacific* 125.926 (2013): 396-408.
- Doyle, J.C. "Analysis of Feedback Systems with Structured Uncertainties", *IEE proceedings*, vol. 129, Parte D, n 6, pp. 242-250, nov. 1982.
- J. J. Da Cruz, "Controle Robusto Multivariável", Edusp, São Paulo, SP, 1996.

11. RESPONSIBILITY NOTICE

The authors are the only responsible for the printed material included in this paper.

APPENDIX 1.

a. Fabry-Perót space state sixth order model matrix definition:

$$A = \begin{bmatrix} 0 & 1 & 0 & 0 & 0 & 0 \\ -\frac{ka+kb+kc}{M} & -\frac{ca+cb+cc}{M} & -\frac{ka-kc}{M}r\frac{\sqrt{3}}{2} & -\frac{ca-cc}{M}r\frac{\sqrt{3}}{2} & -\frac{ka}{2}-\frac{kb}{2}+\frac{kc}{2} & -\frac{ca}{2}-\frac{cb}{2}+\frac{cc}{2} \\ 0 & 0 & 0 & 1 & 0 & 0 \\ -\frac{ka-kc}{I_y}r\frac{\sqrt{3}}{2} & -\frac{ca-cc}{I_y}r\frac{\sqrt{3}}{2} & -\frac{ka+kc}{I_y}r^2\frac{3}{4} & -\frac{ca+cc}{I_y}r^2\frac{3}{4} & -\frac{ka-kc}{I_y}r^2\frac{\sqrt{3}}{4} & -\frac{ca-cc}{I_y}r^2\frac{\sqrt{3}}{4} \\ 0 & 0 & 0 & 0 & 0 & 1 \\ -\left(\frac{ka}{2}-\frac{kb}{2}+\frac{kc}{2}\right) & -\left(\frac{ca}{2}-\frac{cb}{2}+\frac{cc}{2}\right) & -\frac{ka-kc}{I_z}r^2*\frac{\sqrt{3}}{4} & -\frac{ca-cc}{I_z}r^2\frac{\sqrt{3}}{4} & -\frac{ka}{4}+\frac{kb}{4}+\frac{kc}{4}r^2 & -\frac{ca}{4}+\frac{cb}{4}+\frac{cc}{4}r^2 \end{bmatrix}$$

$$B = \begin{bmatrix} \frac{ca}{M} & \frac{cb}{M} & \frac{cc}{M} \\ -\frac{ca+cb+ccc}{M} & -\frac{ca-cc}{M}r\frac{\sqrt{3}}{2} & -\frac{ca+cb+ccc}{M}r\frac{\sqrt{3}}{2} & -\frac{ca-cb+cc}{M}r & \frac{ca}{M} & \frac{ca+ka}{I_z} \\ -\frac{ca+cb+ccc}{M} & -\frac{ca-cc}{M}r\frac{\sqrt{3}}{2} & -\frac{ca+cb+ccc}{M}r\frac{\sqrt{3}}{2} & -\frac{ca-cb+cc}{M}r & \frac{ca}{M} & \frac{ca+ka}{I_z} \\ \frac{ca+ka}{I_z} & 0 & \frac{ca+ka}{I_z} & \frac{ca+ka}{I_z} & \frac{ca+ka}{I_z} & \frac{ca+ka}{I_z} \\ \frac{ca-cc}{I_y}r\frac{\sqrt{3}}{2} & -\frac{ca+cc}{I_y}r^2\frac{3}{4} & -\frac{ca-cc}{I_y}r\frac{\sqrt{3}}{2} & -\frac{ca+cc}{I_y}r^2\frac{3}{4} & -\frac{ca-cc}{I_y}r\frac{\sqrt{3}}{2} & -\frac{ca+cc}{I_y}r^2\frac{3}{4} \\ \frac{ca}{I_z} & -\frac{cb}{I_z} & \frac{ca}{I_z} & -\frac{cb}{I_z} & \frac{ca}{I_z} & -\frac{cb}{I_z} \\ -\frac{ca}{I_z} & -\frac{cb+cc}{I_z} & -\frac{ca-cc}{I_z}r\frac{\sqrt{3}}{4} & -\frac{ca+cb+cc}{I_z}r^2 & -\frac{ca}{I_z} & -\frac{cb+cc}{I_z} \\ -\frac{ca}{I_z} & -\frac{cb+cc}{I_z} & -\frac{ca-cc}{I_z}r\frac{\sqrt{3}}{4} & -\frac{ca+cb+cc}{I_z}r^2 & -\frac{ca}{I_z} & -\frac{cb+cc}{I_z} \end{bmatrix}$$

$$C = \begin{bmatrix} 1 & 0 & r*\frac{\sqrt{3}}{2} & 0 & -\frac{r}{2} & 0 \\ 1 & 0 & -r*\frac{\sqrt{3}}{2} & 0 & -\frac{r}{2} & 0 \\ 1 & 0 & 0 & 0 & -\frac{r}{2} & 0 \end{bmatrix}$$

b. Fabry-Perót system model transfer function representation:

$$G_{11} = \frac{-0.7765s^5 - 3.378 \times 10^4 s^4 - 7.549 \times 10^6 s^3 - 1.661 \times 10^{11} s^2 - 1.345 \times 10^{13} s - 2.004 \times 10^{17}}{s^6 + 163.4s^5 + 7.311 \times 10^6 s^4 + 7.79 \times 10^8 s^3 + 1.742 \times 10^{13} s^2 + 9.014 \times 10^{14} s + 1.342 \times 10^{19}}$$

$$G_{12} = \frac{0.6612s^5 + 2.875 \times 10^4 s^4 + 5.228 \times 10^6 s^3 + 1.161 \times 10^{11} s^2 + 6.726 \times 10^{12} s + 1.002 \times 10^{17}}{s^6 + 163.4s^5 + 7.311 \times 10^6 s^4 + 7.79 \times 10^8 s^3 + 1.742 \times 10^{13} s^2 + 9.014 \times 10^{14} s + 1.342 \times 10^{19}}$$

$$G_{13} = \frac{-0.7764s^5 - 3.378 \times 10^4 s^4 - 7.409 \times 10^6 s^3 - 1.661 \times 10^{11} s^2 - 1.345 \times 10^{13} s - 2.004 \times 10^{17}}{s^6 + 163.4s^5 + 7.311 \times 10^6 s^4 + 7.79 \times 10^8 s^3 + 1.742 \times 10^{13} s^2 + 9.014 \times 10^{14} s + 1.342 \times 10^{19}}$$

Ana María Molina Arcila, Fábio de Oliveira Fialho, Fernando Orsatti
High Resolution Fabry-Pérot Interferometer – Dynamic System Modeling And Nanopositioning Control System Design

$$G_{21} = \frac{-0.8499s^5 - 3.378 \times 10^4 s^4 - 7.705 \times 10^6 s^3 - 1.661 \times 10^{11} s^2 - 1.345 \times 10^{13} s - 2.004 \times 10^{17}}{s^6 + 163.4s^5 + 7.311 \times 10^6 s^4 + 7.79 \times 10^8 s^3 + 1.742 \times 10^{13} s^2 + 9.014 \times 10^{14} s + 1.342 \times 10^{19}}$$

$$G_{22} = \frac{-0.8499s^5 - 3.378 \times 10^4 s^4 - 7.613 \times 10^6 s^3 - 1.661 \times 10^{11} s^2 - 1.345 \times 10^{13} s - 2.004 \times 10^{17}}{s^6 + 163.4s^5 + 7.311 \times 10^6 s^4 + 7.79 \times 10^8 s^3 + 1.742 \times 10^{13} s^2 + 9.014 \times 10^{14} s + 1.342 \times 10^{19}}$$

$$G_{23} = \frac{0.7237s^5 + 2.875 \times 10^4 s^4 + 5.354 \times 10^6 s^3 + 1.161 \times 10^{11} s^2 + 6.726 \times 10^{12} s + 1.002 \times 10^{17}}{s^6 + 163.4s^5 + 7.311 \times 10^6 s^4 + 7.79 \times 10^8 s^3 + 1.742 \times 10^{13} s^2 + 9.014 \times 10^{14} s + 1.342 \times 10^{19}}$$

$$G_{31} = \frac{-0.6361s^5 + 2.859 \times 10^4 s^4 - 3.377 \times 10^5 s^3 + 1.157 \times 10^{11} s^2 + 1.046 \times 10^{12} s - 1.00 \times 10^{17}}{s^6 + 163.4s^5 + 7.311 \times 10^6 s^4 + 7.79 \times 10^8 s^3 + 1.742 \times 10^{13} s^2 + 9.014 \times 10^{14} s + 1.342 \times 10^{19}}$$

$$G_{32} = \frac{0.5416s^5 - 3.362 \times 10^4 s^4 - 1.833 \times 10^6 s^3 - 1.657 \times 10^{11} s^2 - 7.772 \times 10^{12} s - 2.002 \times 10^{17}}{s^6 + 163.4s^5 + 7.311 \times 10^6 s^4 + 7.79 \times 10^8 s^3 + 1.742 \times 10^{13} s^2 + 9.014 \times 10^{14} s + 1.342 \times 10^{19}}$$

$$G_{33} = \frac{-0.636s^5 - 3.376 \times 10^4 s^4 - 7.109 \times 10^6 s^3 - 1.661 \times 10^{11} s^2 - 1.345 \times 10^{13} s - 2.004 \times 10^{17}}{s^6 + 163.4s^5 + 7.311 \times 10^6 s^4 + 7.79 \times 10^8 s^3 + 1.742 \times 10^{13} s^2 + 9.014 \times 10^{14} s + 1.342 \times 10^{19}}$$

APPENDIX 2.

The LQG/LTR design methodology starts designing a plant, called the target loop that meets the performance requirements using Kalman Filter techniques, choosing a proper μ constant and L matrix.

$$G_{TL} = \frac{1}{\sqrt{\mu}} C (j\omega I - A)^{-1} L$$

Using the algebraic Ricatti equation (ARE) and the chosen value for μ , find the Kalman Filter observer gain matrix H.

$$0 = -A\Sigma - \Sigma A' - LL' + \frac{1}{\mu} \Sigma C' C \Sigma$$

$$H = \frac{1}{\mu} \Sigma C'$$

After the Kalman Filter gain matrix is obtained the recovery process is made. As stated in Doyle (1982), if the system is a square system the **A** and **B** matrices of the system are controllable, the **A** and **C** matrices are observable and the transmission zeros of the system have all negative values, a controller gain matrix can be calculated as:

$$G = \frac{1}{\rho} B' K_p$$

Where $\rho > 0$ and K_p is obtained solving the following ARE:

$$0 = -K_p A - A' K_p - C' C + \frac{1}{\rho} K_p B B' K_p$$

With the compensator gain matrix, G, the compensator K for the target loop is defined as:

$$K(s) = G(sI - A + BG + HC)^{-1} H$$

This compensator is made for the design plant model that had augmented dynamics (three integrators in the input signal). Given that we want to design a compensator for the model of the system we need to include the integrators on the compensator as in:

$$K(s) = K(s) * \frac{I_3}{s} = G(sI - A + BG + HC)^{-1} H * \frac{I_3}{s}$$